

**RERTR 2018 – 39TH INTERNATIONAL MEETING ON
REDUCED ENRICHMENT FOR RESEARCH AND TEST REACTORS**

**NOVEMBER 4-7, 2018
SHERATON GRAND HOTEL AND SPA
EDINBURGH, SCOTLAND**

**Surface Characterization of As-Produced and Oxidized
UMo Atomized Powder.**

F. Housaer, P. Simon, P. Demuyt, O. Tougait
Unité de Catalyse et Chimie du Solide, UMR CNRS 8181, Université de Lille,
Cité Scientifique, F-59650 Villeneuve d'Ascq, France

J. Allenou, B. Stepnik
FRAMATOME, CERCA, SPL, ZI Les Bérauds, 54 avenue de la déportation,
F-26104 Romans-sur-Isère, France

F. Béclin, M. Touzin
Unité Matériaux et Transformations, UMR CNRS 8207, Université de Lille,
Cité Scientifique, F-59650 Villeneuve d'Ascq, France

ABSTRACT

Surface quality of the UMo powder is an important factor for the ZrN coating regarding its adherence and sustainability during the plate fabrication steps as well as during in-pile irradiation. Characterization of the passive layer of centrifugal atomized U-7Mo (U-7 wt.% Mo alloy) powder has been studied by atomic force microscopy, powder X-ray diffraction, scanning electron microscopy and X-ray photoelectron spectroscopy. The particle surface was investigated in as-obtained and oxidized states, this latter state being generated by heating the UMo powder up to 300°C under air. A continuous oxide ring with an apparent width of about 0.2 – 0.6 µm encompasses the interior surface of the UMo particles. It comprises nanostructured UO₂, mostly. The SEM and AFM analyses outline rather similar morphological and topographical features of the surface for both types of powder. The XPS study reveals that the passive (as-received UMo) and oxidized layers at the subsurface have identical chemical composition with uranium ions at the U⁵⁺ and U⁶⁺ oxidation states and molybdenum at the Mo⁶⁺ state. In addition to O²⁻ ions, the O 1s spectra show the presence of hydroxyl ions and water molecules.

1 Introduction

For more than two decades, there are continuous international efforts to qualify the high-density UMo/Al fuels for high power research reactors [1]. One fuel design, mostly developed for European facilities, is dispersion fuel, in which UMo (uranium–molybdenum alloy with Mo content between 7 and 10 wt%) powder is dispersed into pure Al or silicon-modified Al alloy matrix [2]. In-pile irradiation tests at severe conditions revealed that volume diffusion occurs between the UMo fuel and the Al matrix yielding the formation of an interaction layer that contributes to excessive fuel swelling [3]. One possible answer to this deleterious fuel/matrix reactivity is the coating of the UMo particle surface with a diffusion barrier. Up to now, zirconium mononitride (ZrN) is the most promising candidate [4].

The properties of UMo(ZrN) core-shell particles, especially the chemical properties to prevent the formation of undesired phases and the mechanical properties to maintain the coating integrity during the fabrication steps, are strongly influence by the deposition techniques, the operating conditions of the coating, but also by the host-particle features. Beside different characteristics concerning the shape, size, density, composition and purity of the substrate, its surface properties have a substantial effect on the quality of the coating. Major issues are the surface roughness (topography), the surface crystallinity and lattice-matching; point and lattice defects, chemical purity, inclusions and surface energy (surface tension) which strongly affect the binding of the first monolayer (chemical adsorption) as well as the physical adsorption of surrounding gaseous molecules such as O₂, N₂, H₂O, CO₂,

In this paper, are presented the results of the characterization of the upper surface of both as-produced U-7Mo powder obtained by centrifugal process as well as controlled oxidized particles from the same batch. The investigation comprises the surface topography by AFM and SEM, the crystallinity by powder XRD diffraction and the elemental composition by XPS analyses.

2 Materials and Experimental Procedures

U-7Mo powder was produced using a centrifugal disk atomizer [5], and was analyzed in as-received (stored in an Ar-glove-box) and oxidized states. Controlled surface oxidation has been monitored using a SETARAM 92 Differential Thermal Analyses system by heating the samples on air up to 300°C. The chemical and physical characterizations were performed on free particles dispersed on graphite tape and on dispersed particles embedded into Al-compacts which were further polished.

SEM images were collected using a JEOL JSM-7800F LV using backscattered and secondary electron modes on free powder and compacts. Chemical analyses were performed using an Oxford Instruments SDD detector (AZTEC 80 mm² spectrometer) for EDS microanalysis. Working distance was set to 10 mm and voltage was adjusted between 5-15kV.

XRD diagrams were collected at room temperature with a D8 Advance Bruker diffractometer (Θ - Θ mode, CuK α radiation) equipped with a LynX'Eye detector. Each diagram was recorded in the range 20-100° (2 Θ), with a step of 0.001° and with a speed of 0.5 s/step. Profile matching and Rietveld analyses were carried out using Fullprof software [6].

The X-ray photoelectron spectroscopy (XPS) experiments were carried out in a Kratos

AXIS Ultra DLD spectrometer using a monochromatic Al $K\alpha$ radiation (1486.6 eV) operating at 225 W (15 mA, 15kV). High-resolution spectra were collected using an analysis area of $\approx 300\mu\text{m} \times 700\mu\text{m}$ and a 20 eV pass energy. Instrument base pressure was 4×10^{-10} Torr. The Kratos charge neutralizer system was used for all analyses and the binding energies were corrected taking C 1s peak corresponding to C-C/C-H type bonding at 284.8 eV as reference. The C 1s, O 1s, Mo 3d and U 4f spectra were analyzed using the CasaXPS software (version 2.3.16, Casa Software Ltd.). Spectra decomposition was performed after a Shirley type background subtraction and Gaussian-Lorentzian profiles with 30/70 Gaussian/Lorentzian proportion were used.

AFM images were collected with a help of Veeco Dimension 3100 Atomic Force Microscope in tapping mode at a constant force of 5-50 pN and with a free oscillation amplitude of 50 nm and a silicone probe Bruker RTESPA-300. Scan sizes were limited to 20 μm .

3 Results

3.1 Cross-section images

Fig.1 shows the cross-section images of both as-received and oxidized U-7Mo powders. The as-received particles present the absence of a detectable oxide layer whereas a continuous layer with a width of about 0.2-0.6 μm is visible on the oxidized particles. The images also outline the evolution of the U-7Mo microstructure from a cellular grain structure for the as-received particles to a rather acicular one for the oxidized particles.

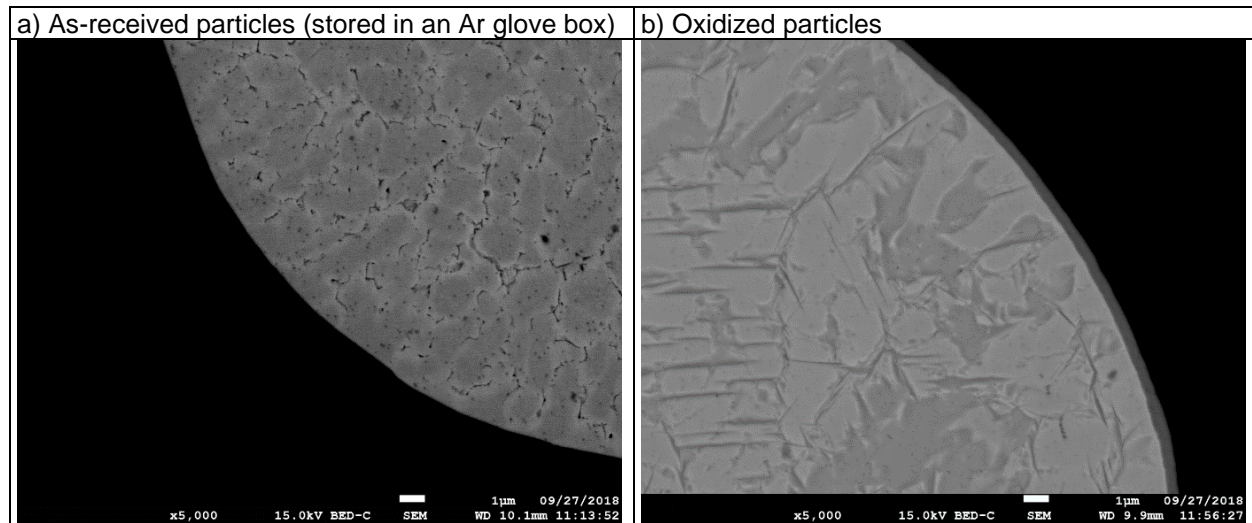


Figure 1 : Cross-section SEM images in BSE mode of a) as-received U-7Mo powder and b) oxidized U-7Mo powder

3.2 Surface examination by AFM and SEM.

The AFM images were recorded using the tapping mode over a surface of 20 x 20 μm^2 allowing to restrict the curvature effect below the amplitude limits. Fig. 2 displays both the AFM and SEM images of the surface of as-received and oxidized U-7Mo particles. The examination of the surfaces reveals rather similar morphological features for both types of powders. The surfaces are heterogeneous (duplex) with areas of well-defined grain structure composed of equiaxed grains of about 1 μm and areas with chaotic

microstructure displaying submicronic grains with blurred separations. The main difference between the two types of particle occurs in the organized zones which shows less sharp grain boundaries in the case of the oxidized particles compared to the as-received one.

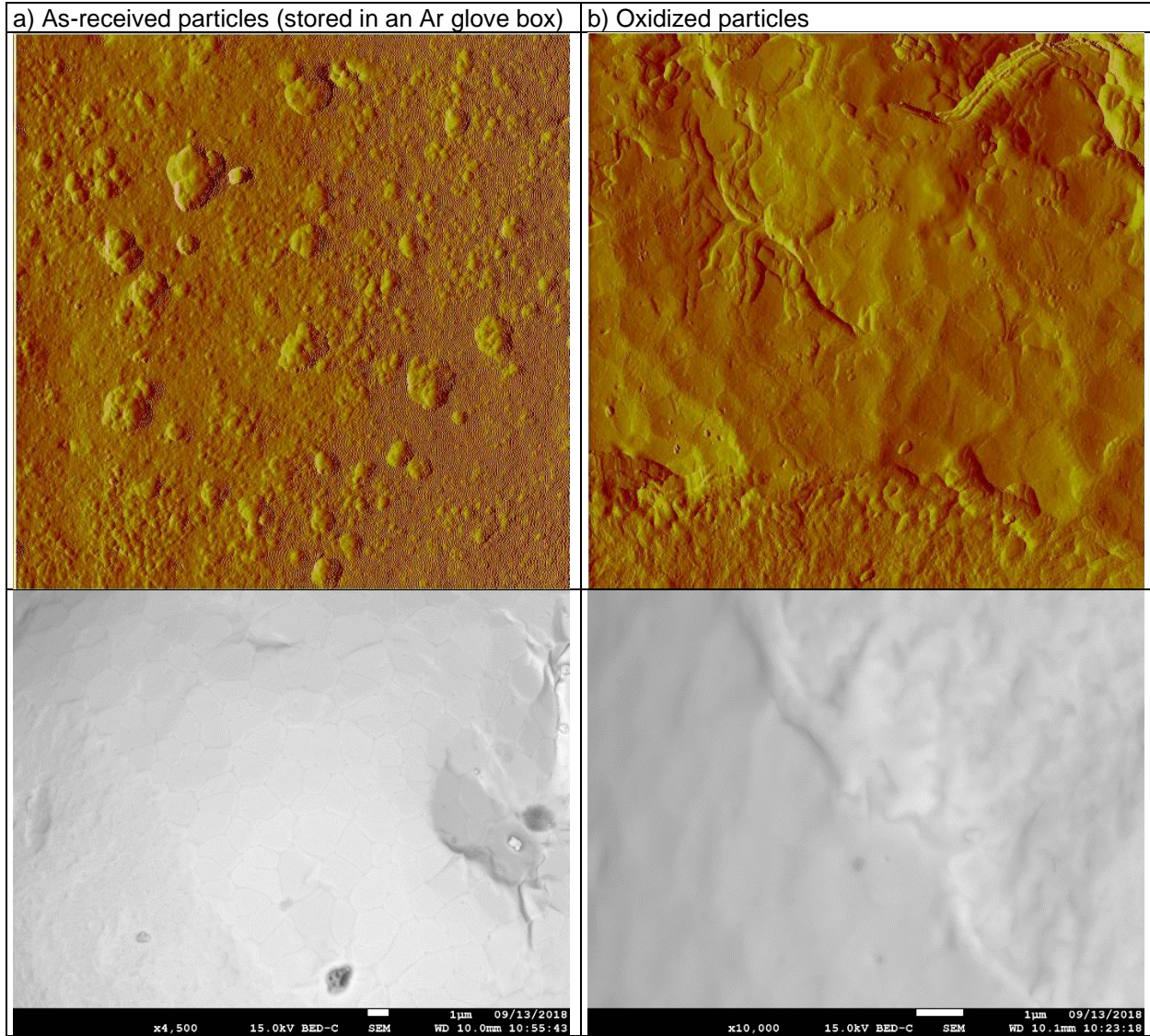


Figure 2 : AFM (20 x 20 μm^2) and SEM images of a) as-received U-7Mo powder and b) oxidized U-7Mo powder

As illustrated on the SEM image of the as-received particle, the U-7Mo atomized powder displays shape deviation from perfect spheres, mainly as hollows which can be associated to solidification shrinkage. The roughness of the U-7Mo particles was directly evaluated on the free powder surface of the as-received and oxidized powders. Three main parameters were picked out to characterize the roughness, R_a , the average value of contours ($R_a = \frac{1}{L} \int_0^L |y| dx$), R_q , the root mean square value of contour ($R_q = \sqrt{\frac{z_1^2 + z_2^2 + \dots + z_n^2}{n}}$),

and the z range. These figures, given in nm, are 46, 61, 657 and 92, 116, 879 for the as-received and oxidized powders, respectively, outlining similar topological features for both types of particle.

3.3 Phase analyze using powder X-ray diffraction

The X-ray diffraction patterns of the as-received and oxidized U-7Mo powders were fully indexed considering the *bcc* W-type (γ UMo) as single crystallized phase and with two crystallized phases, γ UMo and fluorine type (UO_2), respectively. It should be outlined that refinements with two γ UMo phases, according to chemical segregation at the grain boundaries [7], rapidly converge to a unique model with similar structural parameters. The absence of diffraction line belonging to α U outlines the inhibition of the γ UMo eutectoid decomposition. It is in agreement with the previous characterizations of UMo atomized powders and with the U-Mo *TTT* diagram [7, 8]. The lattice refinements of the cubic γ UMo parameter yield, $a = 3.424(1)$ Å and $a = 3.428(1)$ Å, for the as-received and oxidized powders respectively. These values compare well the expected unit-cell parameter for an UMo alloy with 7 wt. % Mo [9]. The apparent crystallite size, deduced from the automatic fitting using the Scherrer formula, amounts to 196(1) and 223(1) nm for the as-received and oxidized powders respectively. They correspond to typical values for rapidly solidified metallic materials.

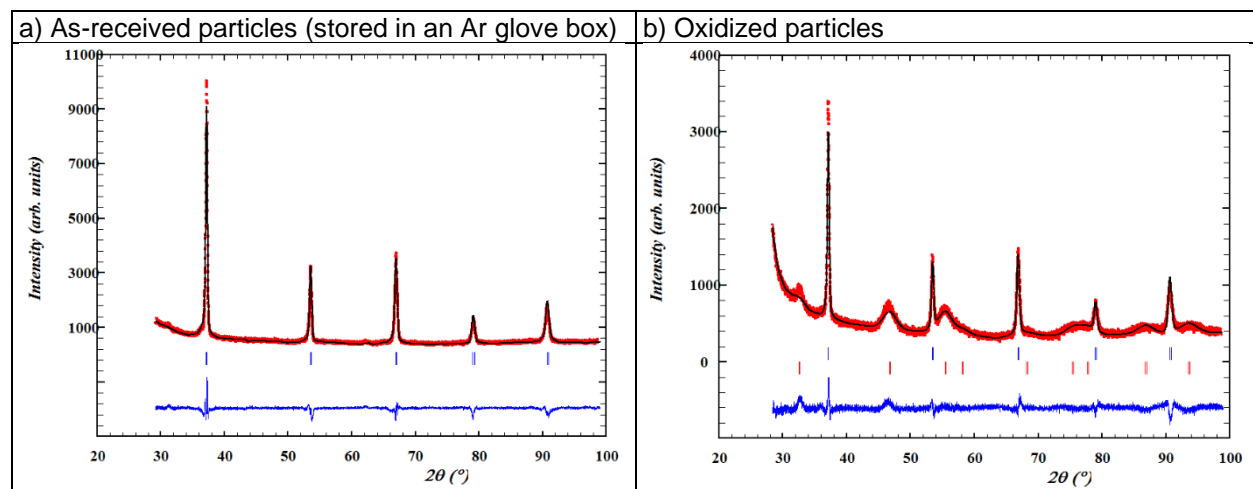


Figure 3: Rietveld plots of a) as-received powder and b) oxidized powder. The blue ticks correspond to the γ UMo phase (cubic, W-type) and the red ticks to UO_2 phase (cubic, CaF_2 -type).

The refined lattice parameter of the fluorine structure, $a = 5.496(1)$ Å compare well the unit-cell parameter of UO_2 . The significant peak broadening was attributed to crystallite smallness. The apparent crystallite size was evaluated to 33(1) nm.

3.4 XPS investigation

XPS survey spectra obtained from the U-7Mo powder in the as-received and oxidized states are given in Fig.4. For both samples, the survey spectra are very similar. They exhibit strong oxygen, uranium and carbon peaks, along with traces of molybdenum and silicon. The presence of Si can be ascribed to a foreign phase with origin remaining

unclear up to now. In the following, only the molybdenum 3d, uranium 4f and oxygen 1s spectra are commented.

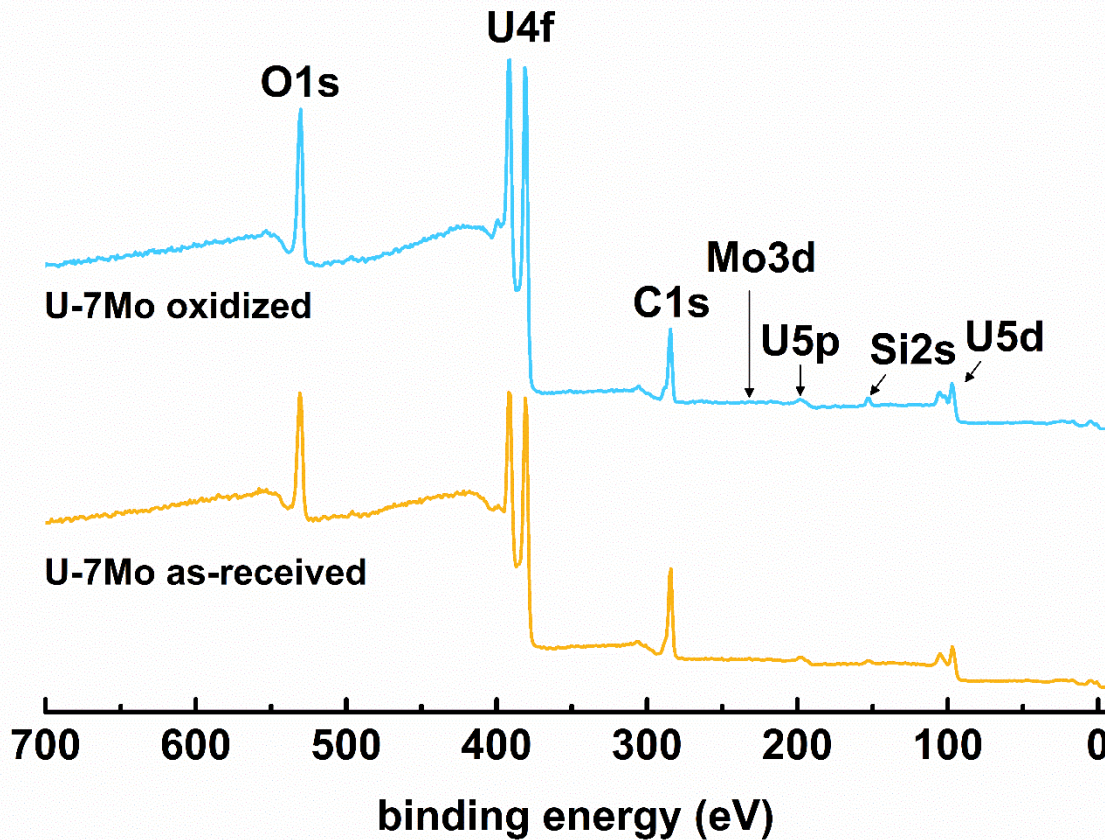


Figure 4 : XPS survey spectra obtained from the U-7Mo powder in the as-received and oxidized states. Each detected photopeak has been labelled on the U-7Mo oxidized powder survey spectrum.

Mo 3d:

Fig. 5 shows the Mo 3d core level spectra for both type of powders. It should be outlined that for both samples, the Mo peaks were not easily discernible despite Mo content of 15.8 at. % (7 wt. % Mo) in the UMo powders. This would indicate that molybdenum is at very low concentration at the surface. In spite of the low signal intensity, it was possible to identify in the spectra a doublet peak, corresponding to Mo 3d_{5/2} and Mo 3d_{3/2}. The Mo 3d_{5/2} contribution is localized at 232.7 eV indicating that the Mo is thus present as Mo⁶⁺ species in both powders. In case of metallic molybdenum, the asymmetric peaks would be located at 227.8(1) eV and 230.9(1) eV for Mo 3d_{5/2} and Mo 3d_{3/2}, respectively [10].

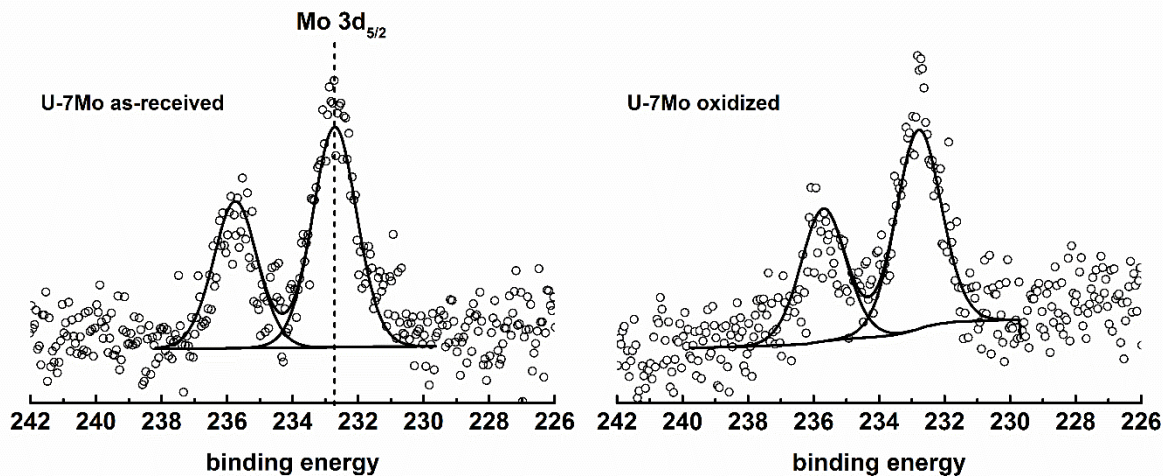


Figure 5: XPS Mo 3d spectra obtained from the U-7Mo powder in the as-received and oxidized states.

U 4f:

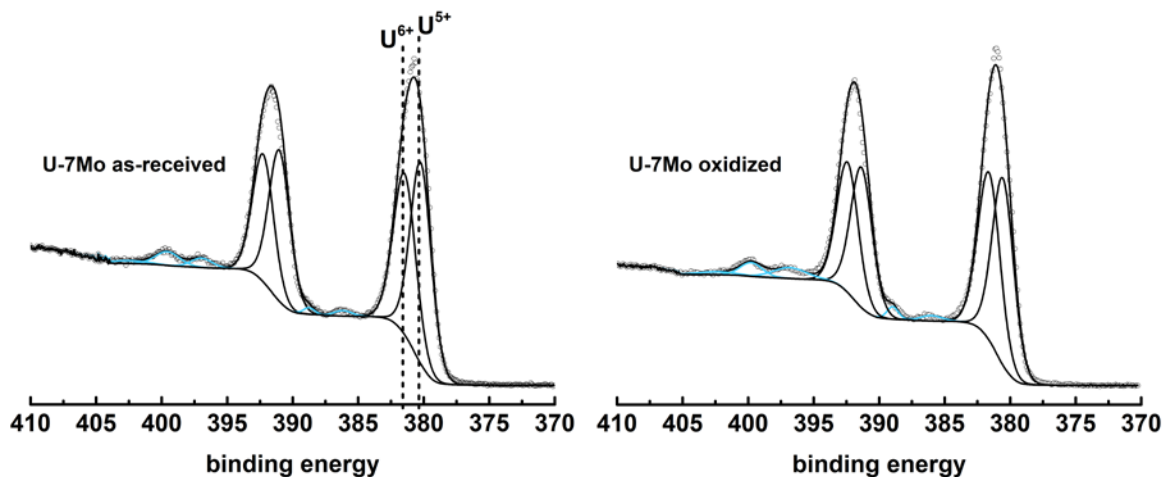


Figure 6: XPS U 4f spectra obtained from the U-7Mo powder in the as-received and oxidized states. The blue contributions correspond to the satellites peaks in the decomposition.

Fig. 6 presents the U 4f XPS core level spectra for as received and oxidized U-7Mo powders. The spectra are dominated by two major contributions localized at 381.1 eV and 391.9 eV which can be attributed to U 4f_{7/2} and U 4f_{5/2} half orbitals. Alongside to these main peaks, two additional small ripples can be found in both U 4f_{7/2} and U 4f_{5/2} parts of the spectra, corresponding to satellite peaks. In order to determine the oxidation state of uranium, a careful examination of the satellite-primary peak binding energy separation was undertaken, based on Ilton *et al.* [11] and Gouder and coworkers [12, 13] works. The presence of one satellite peak located above the primary lines, arising from shakeup or charge transfer process, is well documented for U(IV) and U(V) compounds, whereas the presence of two satellites peaks has been observed for the U(VI) compounds. Thus, the presence of two satellites peaks in the spectra seems to indicate that uranium is present at the surface as U(VI). However, U(VI) compounds usually display satellite peaks at about 4 eV and 10 eV above the primary lines, with a U 4f_{7/2} “10 eV” satellite

buried under the primary U 4f_{5/2} line. We therefore assume that due to the presence of two visible satellite peaks in the U 4f_{7/2} part of the spectra, uranium is present at the surface in a mixed-valence state, with at least two oxidation state.

The U 4f_{7/2} and U 4f_{5/2} primary lines were thus fitted with two components, corresponding to two different oxidation states. These components lie respectively at a BE of 380.55 eV and 381.6 eV, with a full width at half maximum (FWHM) of 1.9(1) eV and a spin orbit splitting of 10.8 eV.

The satellite structures were fitted with two peaks in the U 4f_{7/2} part of the spectra. The first satellite peak is located at 8.5 eV above the first primary line. The satellite peak position, together with the primary line BE suggests that the first component corresponds to U(V) species. The second satellite peak is located at 4.7 eV above the second primary line. This low satellite-primary peak binding energy separation is only found for U(VI) species. That, along with the primary line BE, indicates that the second species at as received and oxidized U-7Mo powders surfaces is U(VI).

O 1s:

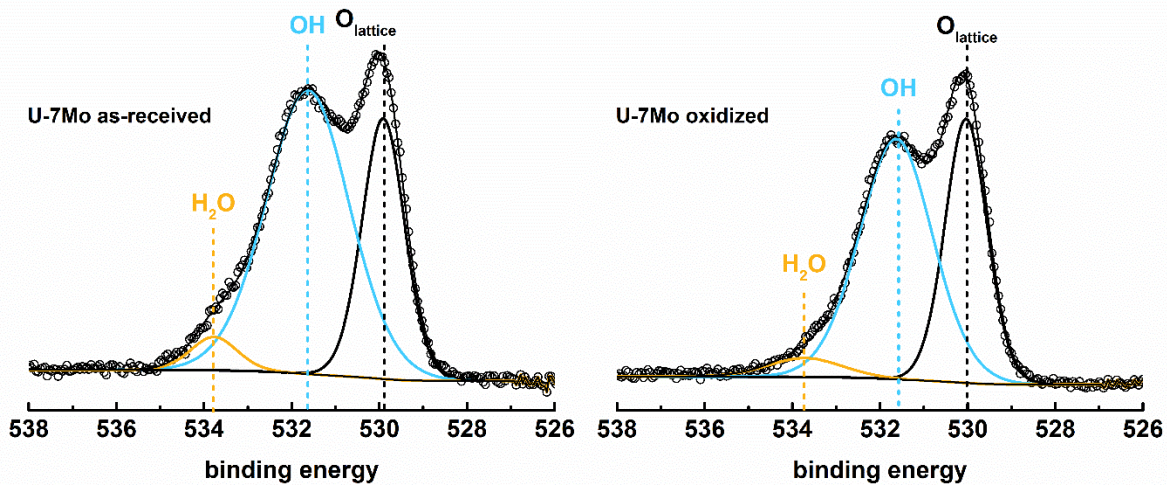


Figure 7 : XPS O 1s spectra obtained from the U-7Mo powder in the as-received and oxidized states.

The O 1s core level spectra for as received and oxidized U-7Mo powders are presented in Fig. 5. For both UMo powders, the spectra are dominated by an oxide peak at 530.0(1) eV and a OH⁻ peak at 531.6(1) eV. Both spectra exhibit a shoulder at high BE (533,7(1) eV) which corresponds to adsorbed water.

4 Conclusion

The subsurface and outer surface of as-received and oxidized U-7Mo atomized particles were analyzed by means of SEM, AFM, powder X-ray diffraction and XPS. The controlled oxidization of the particles was performed by heating the U-7Mo powder at 10°C/min up to 300°C under air. The oxide layer developed as a shell at the outer surface with an apparent width ranging from 0.2 to 0.6 μm. It comprises UO₂ with nanosized crystallites. Both types of powder display similar morphological and topographical surface features. They can be classified as rather smooth with some irregularities associated to solidification shrinkage, mainly. They show heterogeneous surface microstructure

composed of areas with well-defined micronic equiaxed grains and areas with chaotic organization of submicronic grains. Chemical characterization of the subsurface was carried out by XPS yielding similar behaviors for both types of powder. It indicates that the passive layer developed on as-received UMo powder and the subsurface of the oxidized layer have identical chemical composition with strong oxygen, uranium and carbon peaks, along with traces of molybdenum and silicon. The present study focuses on the molybdenum 3d, uranium 4f and oxygen 1s spectra only. The Mo contribution which hardly emerges from the background suggests Mo depletion at the subsurface (6 nm deep) where it is present at the Mo⁶⁺ oxidation state. The careful examination of the U 4f spectra with 4f_{5/2} and 4f_{7/2} photopeaks and satellites reveals the presence of uranium ions at the U⁵⁺ and U⁶⁺ oxidation states, only. The analysis of the O 1s spectra show that beside the presence of O²⁻, contribution from hydroxyl ions (OH⁻), and H₂O groups were detected.

Supplementary investigations of the subsurface of both type of powder are currently under way. These new results along with the detailed analyze of the XPS study will be submitted as a manuscript in a peer-reviewed journal.

5 Acknowledgement

Chevreul Institute (FR 2638), Ministère de l'Enseignement Supérieur et de la Recherche, Région Nord – Pas de Calais and FEDER are acknowledged for supporting and funding partially this work.

6 References

- [1] JL Snelgrove, GL Hofman, MK Meyer, CL Trybus, TC Wiencek, "Development of very-high-density low-enriched-uranium fuels", Nuclear Engineering and Design 178 (1997) 119–126.
- [2] S. Van den Berghe, P. Lemoine, "Review of 15 years of high-density low enriched UMo dispersion fuel development for research reactors in Europe", Nuclear Engineering and Technology, 46 (2014) 125-146.
- [3] B. Ye, G.L. Hofman, A. Leenaers, A. Bergeron, V. Kuzminov, S. Van den Berghe, Y.S. Kim, H. Wallin, "A modelling study of the inter-diffusion layer formation in U-Mo/Al dispersion fuel plates at high power", Journal of Nuclear Materials, 499 (2018) 191-203.
- [4] A. Leenaers, S. Van den Berghe, C. Detavernier, "Surface engineering of low enriched uranium–molybdenum", Journal of Nuclear Materials 440 (2013) 220–228.
- [5] K. H. Kim, D. B. Lee, C. K. Kim, G. E. Hofman, K. W. Paik, "Characterization of U-2 wt% Mo and U-10 wt% Mo alloy powders prepared by centrifugal atomization", Journal of Nuclear Materials, 245 (1997) 179-184.
- [6] J. Rodriguez-Carvajal, "Recent Developments of the Program FULLPROF", in Commission on Powder Diffraction (IUCr), Newsletter (2001), 26, 12-19.
- [7] J. M. Park, H. J. Ryu, K. H. Kim, D. B. Lee, Y. S. Lee, J. S. Lee, B. S. Seong, C. K. Kim, M. Cornen, "Neutron diffraction analyses of U-(6–10 wt.%)Mo alloy powders fabricated by centrifugal atomization", Journal of Nuclear Materials 397 (2010) 27–30.
- [8] T. Zweifel, H. Palancher, A. Leenaers, A. Bonnin, V. Honkimaki, R. Tucoulou, S. Van Den Berghe, R. Jungwirth, F. Charollais, W. Petry, "Crystallographic study of Si and ZrN coated U–Mo atomised particles and of their interaction with al under thermal annealing",

Journal of Nuclear Materials, 442 (2013) 124-132.

[9] A. E. Dwight, "The uranium-molybdenum equilibrium diagram below 900° C", Journal of Nuclear Materials, 2, (1960) 81-87.

[10] E. Gardin, S. Zanna, A. Seyeux, A. Allion-Maurer, P. Marcus, Comparative study of the surface oxide films on lean duplex and corresponding single phase stainless steels by XPS and ToF-SIMS, Corrosion Science 143 (2018) 403-413.

[11] E. S. Ilton, J-F Boily, P. S. Bagus, Beam induced reduction of U(VI) during X-ray photoelectron spectroscopy: The utility of the U4f satellite structure for identifying uranium oxidation states in mixed valence uranium oxides, Surface Science 601 (2007) 908–916.

[12] M. Paukov, I. Tkach, F. Huber, T. Gouder, M. Cieslar, D. Drozdenko, P. Minarik, L. Havela, U-Zr alloy: XPS and TEM study of surface passivation, Applied Surface Science 441 (2018) 113–119.

[13] R. Eloirdi, P. Cakir, F. Huber, A. Seibert, R. Konings, T. Gouder, X-ray photoelectron spectroscopy study of the reduction and oxidation of uranium and cerium single oxide compared to (U-Ce) mixed oxide films, Applied Surface Science 457 (2018) 566–571.